Contrib Mineral Petrol (1997) 127: 136–146

Joël Brugger · Reto Gieré · Stefan Graeser
Nicolas Meisser

The crystal chemistry of roméite

Received: 5 March 1996 / Accepted: 18 October 1996

Abstract Roméite (Ca, Fe, Mn, Na)$_2$(Sb^{5+}, Ti^{4+})$_2$(O, OH, F)$_7$ is a rare mineral found in metamorphic iron-manganese deposits and in hydrothermal Sb-bearing veins. It is isostructural with the pyrochlore-group minerals of the general formula $A_{2-m}B_2X_{6-w}Y_{1-n} \cdot pH_2O$. The pyrochlore-group minerals are important Nb and Ta ores, and are also used as an actinide host phase in radioactive waste. The crystal chemistry of roméite from the type locality Praborna (Italy), from Massiac (France), and from four newly discovered localities in the Swiss Alps, and of "lewisite", a questionable species related to roméite from Tripuhy (Brazil), is compared to that of pyrochlore. A wide range of substitutions has been observed including (1) independent substitutions on the A- and B-sites, and (2) coupled substitutions between the A- and B- and between the A- and Y- sites. Only the roméite from Massiac, derived from weathering of stibnite, contains significant H_2O (up to 14 wt%). The A-site vacancies in roméite appear to be controlled by the primary conditions of crystallization, and not by post-crystallization alteration. The Y-site chemistry of roméite varies from locality to locality; it can be dominated by F, OH, or be fully vacant. The "lewisite" octahedral crystals studied are a sub-microscopic mixture of roméite with a mineral structurally related to pyrochlore, which grows at the expense of roméite.

J. Brugger (✉) · R. Gieré[1] · S. Graeser
Institut für Mineralogie und Petrographie,
Universität Basel, Bernoullistr. 30,
CH-4056 Basel. e-mail: brugger@ubaclu.unibas.ch.

N. Meisser
Musée de Géologie et Institut de Minéralogie,
Université BFSH 2, -CH-1015 Lausanne.

Present address:
[1]Department of Earth and Atmospheric Sciences,
Purdue University, West Lafayette, IN 47907-1397, USA

Editorial responsibility: T. Grove

Introduction

Pyrochlore-group minerals (Table 1), the most important Nb and Ta ores, are widespread accessories in a variety of igneous rocks including carbonatites, nepheline syenites and related alkaline rocks, and granitic pegmatites. Synthetic pyrochlore hosts actinides in SYNROC, a promising ceramic material designed for the immobilization of high-level radioactive waste (Ringwood et al. 1988). Studies of the effect of growth and alteration on the crystal chemistry of natural pyrochlore allow the development of models for the long-term stability of such ceramics (Lumpkin and Ewing 1985, 1992, 1996; Lumpkin et al. 1994).

Roméite is isostructural with the pyrochlore-group minerals, but occurs in different geological environments, namely in metamorphic rocks and hydrothermal veins. The comparison of the crystal chemistry of roméite with that of pyrochlore-group minerals in relation to alteration and affinity for trace elements allows a better understanding of the crystal chemistry of the pyrochlores sensu lato. The second aim of this study is to discuss the geological significance of roméite, which was found to be an important accessory mineral in the Fe-Mn ores of Val Ferrera (Switzerland). Roméite displays contrasting chemistry from one deposit to the other, emphasizing the need of a nomenclature able to reflect this variability. Thus, the nomenclatural problems are reviewed, and "lewisite", a questionable species related to roméite, has been reinvestigated.

Roméite and the pyrochlore group

Roméite has been discovered by Damour (1841) in the Praborna mine (Piemont, Italy) and named in honor of French mineralogist Romé de l'Isle (1736–1790). Although the Praborna roméite was originally described as $CaSb_2^{3+}O_4$, a pentavalent oxidation state of Sb was determined by Schaller (1916). After demonstrating that

Table 1 Overview of the pyrochlore group

Structure	space group *Fd3m*, Z = 8; isotype of pyrochlore (as defined by Gaertner 1930 and Brandenberger 1931)			
General formula	$A_{2-m}B_2X_{6-w}Y_{1-n} \cdot pH_2O$			
Chemistry	A	B[a]	X	Y
	Ca^{2+}	**Nb^{5+}**	O^{2-}	OH^-
	Na^+	**Ti^{4+}**		F^-
	Ba^{2+}	**Ta^{5+}**	F^{-a}	O^{2-}
	Bi^{2+}	W^{5+}	OH^{-c}	
	U^{4+}	Sb^{5+}		K^{+b}
	REE^{3+}	Fe^{3+}		Rb^{+b}
	Y^{3+}	Al^{3+}		Cs^{+b}
	Th^{4+}	...		Tl^{+b}
	Zr^{4+}			...
	Sb^{3+}			
	Pb^{2+}			
	...			
Site occupancy	m:	0 (*ideal pyrochlore*) to 2 (*defect pyrochlore*)		
	w:	normally 0; however Lumpkin and Ewing (1992) describe limited vacancy on this site;		
	n:	0–1		
	p:	< 2; *H_2O-groups occur on the A- and Y-sites*		

[a] In the official mineralogical classification, only pyrochlores with Nb, Ta or Ti dominant on B-site are assigned to the "pyrochlore group".
[b] A pyrochlore in which a large monovalent cation occurs on the Y-site is called *inverse pyrochlore*.
[c] F^- and OH^- rarely, only in limited amounts.

roméite is isostructural with pyrochlore, Zedlitz (1932) described roméite with the presently accepted chemical formula $(Ca, Fe, Mn, Na)_2(Sb^{5+}, Ti^{4+})_2(O, OH, F)_7$.

Before the chemical composition and structure of roméite had been clearly established, several Sb-minerals related to roméite were described under various names. Dana and Dana (1951), however, considered the following minerals as roméite varieties: atopite (sodian and manganoan), schneebergite (ferroan), lewisite (titanian), mauzeliite (plumbian), weslienite (fluorian), and hydroroméite (up to 13.48 wt% H_2O, Natta and Baccaredda 1933). Roméite and "lewisite" are still listed as independent species in most current reference manuals (e.g., Fleischer 1993), although the chemical analysis of "lewisite" given by Hussak and Prior (1895) for the sample from the type locality Tripuhy (Brazil) corresponds to titanian roméite. Pyrochlore-related minerals have the general chemical formula $A_{2-m}B_2X_{6-w}Y_{1-n} \cdot pH_2O$ (see Table 1 for details). According to the *crystallographic* classification, all phases isostructural with pyrochlore belong to the pyrochlore group; we will refer to this point of view as pyrochlore sensu lato (s.l.). The *mineralogical classification* is, according to the IMA Subcommittee on Nomenclature of the Pyrochlore Group (Hogarth 1977), more restrictive because only compounds with Nb (pyrochlore subgroup), Ta (microlite subgroup) or Ti (betafite subgroup) as main B-cations are assigned to the pyrochlore group; we will refer to the latter as pyrochlore sensu stricto (s.s.). The name of each species is given by the name of the subgroup accompanied by a prefix that indicates the main A-cation (e.g., plumbopyrochlore).

There are three main flaws to the IMA classification. (1) Isostructural minerals with Sb and W as dominant B-site cations (i.e., stibiconite-group and ferritungstite-group, respectively) were not taken into account; this simplification may reflect the fact that these minerals occur in very different geological environments. (2) Vacancies on the A-site play an important role in pyrochlore s.l. (Table 1), another aspect that is not taken into account by the mineralogical classification. (3) H_2O groups can be predominant on the A-site, as shown for kalipyrochlore (Ercit et al. 1994) and ferritungstite (Ercit and Robinson 1994). K, from which kalipyrochlore (2 wt% K_2O) received its name (Van Wambeke 1978), does not occur on the A-site but rather on the Y-site (see Table 1).

Analytical procedures

Polished thin sections (30 μm thick) were obtained when the abundance of roméite within the rock was sufficient. Roméite grains from Fianel, Tripuhy and Massiac, isolated under the binocular microscope, were embedded in an epoxy resin and then polished. In each grain, the chemical zonation was studied using back scattered electron (BSE) images. In roméite, this method basically maps the substitution of Sb by Ti due to the large difference in atomic number (51 and 22 respectively); Ti-rich zones appear darker than Sb-rich zones.

Quantitative electron microprobe (EMP) analyses were performed with a JEOL JXA-8600 at the Institute of Mineralogy and Petrography at the University of Basel, under the following analytical conditions: 10 nA (beam current on a Faraday cage), 15 kV, scanning mode (analyzed surface ≈ 20 μm^2), and ZAF correction. The following standards, X-ray lines and detector crystals were used: wollastonite (Ca-K_α/PET), albite (Na-K_α/TAP, Al-K_α/TAP), valentinite (Sb-L_α/PET), rutile and kaersutite (Ti-K_α/PET), graftonite (Mn-K_α/LiF and Fe-K_α/LiF), adamite (As-K_α/LiF), CeO_2 (Ce-L_α/LiF), metallic Nb (Nb-L_α/PET), metallic U (U-M_α/PET), galena (Pb-M_α/PET), scheelite (W-L_α/LiF), and topaz (F-K_α/LDE1).

Table 2 Selected EMP analyses of roméite[a]

Analysis N°	1	2	3	4	5	6	7	8	9	10	11	12	13	14	15
Deposit	Praborna	Fianel	Fianel	Fianel	Fianel	Fianel	V. Sterla	V. Sterla	Starlera	Starlera	Schmor.	Schmor.	Tripuhy	Tripuhy	Massiac
Points[b]	7	15	5	3	3	3	5	6	12	8	12	4	7	7	1
Sb_2O_5	75.41	66.63	68.42	73.60	55.50	30.14	65.24	76.03	76.34	67.87	68.49	60.42	66.11	70.25	77.01
TiO_2	< 0.03	6.26	6.81	2.83	12.22	18.44	8.26	0.98	< 0.03	5.97	0.58	1.03	13.06	7.20	< 0.03
Nb_2O_5	0.02	0.19	0.06	0.02	0.39	0.52	0.15	0.11	0.03	0.20	0.05	0.10	0.16	0.07	
Al_2O_3											0.02	0.03	0.53	1.14	
Fe_2O_3											2.31	3.10	3.65	5.66	
FeO	0.76	0.14	0.03	0.06	0.55	1.59	0.16	0.41	0.49	0.13					0.16
As_2O_5					0.81	4.73			0.04	< 0.03	0.34	2.10	0.18	0.34	
WO_3					0.19	3.11									
Ce_2O_3	0.04	0.61	0.02	0.01	1.61	0.27	1.46	0.05	0.03	1.22	0.06	0.16	< 0.01	< 0.01	0.10
Na_2O	0.97	4.00	1.97	1.35	2.08	1.01	4.26	6.08	6.28	4.72	1.42	1.16	0.22	0.12	0.70
CaO	17.98	18.79	20.80	19.40	16.93	7.88	19.26	15.16	14.56	17.65	16.23	15.27	15.95	15.35	9.28
MnO	2.51	0.22	0.58	1.08	0.45	0.31	0.15	0.06	0.09	0.46	5.87	6.21	0.60	0.25	< 0.03
UO_2					3.30	17.37									
PbO					< 0.05	8.65									
F	0.76	4.49	2.49	1.99	2.70	0.16	4.34	4.41	4.21	3.85	1.29	0.87	< 0.05	< 0.05	< 0.05
OH	2.17														
−(OH,F)	1.34[c]	1.89	1.05	0.84	1.14	0.07	1.83	1.86	1.77	1.62	0.54	0.37	0.00	0.00	
Sum	99.28	99.44	100.13	99.50	95.59	94.11	101.46	101.43	100.30	100.45	96.11	90.08	100.46	100.38	87.25
Normalisation Σ(B-cations) = 2															
Sb	1.999	1.675	1.663	1.855	1.353	0.784	1.588	1.946	1.997	1.692	1.827	1.680	1.295	1.398	2.000
Ti	0.000	0.319	0.335	0.144	0.604	0.971	0.407	0.051	0.000	0.302	0.031	0.058	0.518	0.290	0.000
Al											0.002	0.002	0.033	0.072	
Fe^{3+}											0.125	0.175	0.145	0.228	
Nb	0.001	0.006	0.002	0.001	0.012	0.016	0.005	0.003	0.001	0.006	0.002	0.003	0.004	0.002	
As					0.028	0.173			0.002	0.000	0.013	0.082	0.005	0.010	
W					0.003	0.056									
Σ(B)	2.000	2.000	2.000	2.000	2.000	2.000	2.000	2.000	2.000	2.000	2.000	2.000	2.000	2.000	2.000
Na	0.135	0.524	0.250	0.178	0.265	0.137	0.542	0.812	0.858	0.614	0.198	0.169	0.023	0.013	0.095
Ca	1.375	1.364	1.458	1.411	1.191	0.591	1.353	1.119	1.099	1.269	1.249	1.224	0.901	0.881	0.695
Fe^{2+}	0.045	0.008	0.002	0.003	0.030	0.093	0.009	0.024	0.029	0.008					0.009
Mn	0.151	0.012	0.032	0.062	0.025	0.019	0.008	0.003	0.005	0.026	0.357	0.393	0.027	0.011	0.000
Pb					0.000	0.163									
U					0.048	0.271									
Ce	0.001	0.015	0.001	0.000	0.039	0.007	0.035	0.001	0.001	0.030	0.001	0.004	0.000	0.000	0.003
Σ(A)	1.707	1.923	1.743	1.654	1.598	1.281	1.947	1.959	1.992	1.947	1.805	1.790	0.951	0.905	0.802
F	0.172	0.962	0.514	0.428	0.561	0.035	0.900	0.962	0.937	0.817	0.292	0.205	0.000	0.000	0.000
OH	0.547														
Y[]max[d]		0.010	0.292	0.293	0.487	0.953	0.060	–	–	0.087	0.290	0.396			
O	6.281	6.028	6.194	6.279	5.952	6.012	6.040	6.047	6.095	6.096	6.418	6.399	5.503	5.454	5.756
(O,OH,F)	7.000	6.990	6.708	6.707	6.513	6.047	6.940	7.009	7.032	6.913	6.710	6.604	5.503	5.454	5.756

[a] Sample description: (1) Sample MGL37726 from *Praborna*, *Piemont*, *Italy*. (2) Grain *FI10/c*, *Fianel*, *Val Ferrera*. (3) BSE dark zones of grain *Se2.3*, *Fianel*, *Val Ferrera*. (4) BSE light zones of grain *Se2.3*, *Fianel*, *Val Ferrera*. (5) BSE dark, heterogeneous parts of the crystal *Se2/4*, *Fianel*, *Val Ferrera*. 1.85 wt% H_2O required to fill the A-site. (6) Betafite in the core of the roméite crystal *FI10/D*, *Fianel*, *Val Ferrera*. 3.21 wt% H_2O required to fill the A-site. (7) BSE darkest regions in the crystal of Fig. 4b (*Val Sterla*, *Val Ferrera*). (8) BSE lightest regions in the crystal of Fig. 4b (*Val Sterla*, *Val Ferrera*). (9) "Ti-free" roméite from *Starlera*, *Val Ferrera*. (10) "Ti-rich" roméite from *Starlera*, *Val Ferrera*. (11) Homogeneous parts of three roméite crystals from sample *JB337*, *Schmorrasgrat*, *Val Ferrera*. (12) Thin (< 1 μm), BSE dark zones of roméite from sample *JB337*, *Schmorrasgrat*, *Val Ferrera*. The As_2O_5-content is highly variable (0.13 to 6.16 wt%). (13) Grain n° 1 from *Tripuhy*, *Brazil*. (14) Grain n° 2 from *Tripuhy*, *Brazil*. (15) Roméite from *Massiac*, *France*.

[b] Number of analyses averaged.

[c] Calculated on the basis of 7 (O + OH + F).

[d] (Y[]max) maximum number of vacancies on the Y-site based on 7 (O + F + Y[]).

Because of a strong interference between Sb-L_α and As-L_α, the K_α-line was chosen for As despite its poor excitation at 15 kV. Under the conditions chosen for background measurement, the effect of the Ca-K_α line on the Sb-L_α line is not significant, and conversely, not more than +0.5% of the Ca-K_α intensity is due to interference with the Sb-L_α line. All other possible interferences were tested and found negligible, in particular the Ce-L_α – Ti-K_β interference. The intensity of F-K_α in roméite does not vary significantly during the first 60 seconds of electron bombardment (Stormer et al. 1993). File handling and all calculations with the analytical data were performed with Petrocalc (Godard and Chat 1994).

IR spectra were obtained with a Perkin-Elmer 883 infrared photometer using KBr pills. Gandolfi and Guinier-Hagg cameras furnished the X-ray powder data, and Weissenberg and precession devices the single crystal data for "lewisite".

Geology, morphology and chemistry of roméite

Praborna

A syngenetic exhalative Fe-Mn mineralization is embedded in radiolarites deposited on the Mesozoic pillow lavas of the oceanic "Nappe Piémontaise" at Praborna (Val d'Aoste, Italy). The ores underwent a polyphase Alpine metamorphism (Martin-Vernizzi 1984) evolving from a blueschist phase into a climax under eclogitic conditions ($P = 10$ kbar, $T = 465 \pm 15$ °C), and finally to a retrograde greenschist-facies stage. Yellow to brownish octahedral roméite crystals up to 1 mm in size occur in late calcite veinlets crosscutting piemontite-rich layers.

These roméites are TiO_2-free (< 0.04 wt%; cf. Table 2, analysis 1). Limited substitution of Na, Fe and Mn for Ca is observed on the A-site which exhibits a mean occupancy of 1.707. The Y-site contains not more than 0.2 atoms of F pfu. A predominance of hydroxyl over F and O on this site is indicated by the low sums of the EMP analyses and also by a sharp absorption corresponding to OH vibrations on the IR-spectrum (arrow in Fig.1a).

The substitution $^{A}Na_3^{Y}(OH)^{A}(M^{2+})_{-2}{}^{A}\square_{-1}{}^{Y}O_{-1}$ relates the formula obtained in this study to the formula $CaNaSb_2^{5+}O_6(OH)$ proposed by Zedlitz (1932). A set of independent exchange vectors important to explain the chemical variability of the samples studied is listed in Table 3; the above substitution is a linear combination of the substitutions (a) $M^{2+}\square Na_{-2}$ and (c) $^{A}Na^{Y}(OH)^{A}(M^{2+})_{-1}{}^{Y}O_{-1}$, where M^{2+} = (Ca, Mn, Fe).

Val Ferrera

Numerous small Fe and Fe-Mn deposits (Stucky 1960; Brugger 1995) are embedded in the Triassic marbles of the Middle Penninic Suretta and Schams Nappes (Trümpy 1980) in Val Ferrera (Central Alps; Graubünden, Switzerland). A synsedimentary exhalative origin of these deposits is suggested by Brugger (1996); their present mineral assemblage was formed during a polyphase Tertiary metamorphism (Schmid et al. 1990; Schreurs 1993), evolving from a blueschist phase (> 10 kbar, < 350 °C, 50 Ma) to an upper greenschist phase (< 10 kbar, 350 °C < T < 450 °C, 35–40 Ma) associated with a pervasive schistosity (S_1), and finally to a lower greenschist phase (> 5 kbar, < 450 °C, $30 < t <$ 35 Ma). Several abandoned mine sites were examined including Fianel, Schmorrasgrat, Starlera, and Val Sterla.

At the *Fianel* mine (Suretta nappe), roméite occurs scarcely in syn-kinematic quartz veinlets within a stratabound lens (1 m × 0.5 m) of pink dolomitic breccia enclosed in hematite, quartz, carbonate, ±barite, ±fluorapatite ores, together with beryl, scheelite-powellite, paraniite-(Y) and bergslagite (Brugger et al. 1994, 1995). The roméite crystals are fractured, whereby the sutures are filled with quartz (Fig. 2a,b,c). On the BSE images, most of the roméite crystals have a homogeneous appearance, but sometimes exhibit a dark (Ti-rich) rim, which may contain tiny thorian monazite-(Ce) inclusions (Fig. 2a). Rarely, they show inclusions of Ti-rich roméite, which display a myrmekitic appearance. One crystal, sample Se2.3, is unusual because of its fine oscillatory zonation (Fig. 2b). The rim of the crystal shown in Fig. 2c also displays a fine oscillatory zonation which, however, is not parallel to the crystal faces; the core is constituted of heterogeneous betafite. The crystal surfaces of betafite and the enclosing roméite are generally parallel, suggesting epitaxial growth. Note that on one side the betafite crystal was dissolved before roméite crystallized.

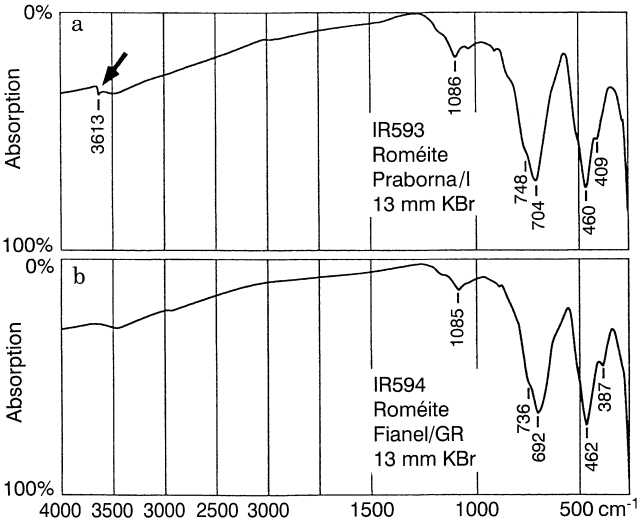

Fig. 1 IR spectra of roméite from **a** Praborna, Italy and **b** Fianel, Val Ferrera, Switzerland. The *arrow* points to the absorption resulting from OH vibration

Table 3 Important exchange vectors for the roméites described in this study

(a)	$^{A}Ca^{A}\square{}^{A}Na_{-2}$
(b)	$^{A}\square{}^{B}Sb_2{}^{A}Ca_{-1}{}^{B}Ti_{-2}$
(c)	$^{A}Na^{Y}(OH)^{A}M^{2+}_{-1}{}^{Y}O_{-1}$
(d)	$^{A}Ce^{B}Ti_2{}^{A}Na_{-1}{}^{B}Sb_{-2}$
(e)	$^{B}Sb^{5+}{}^{B}(Fe^{3+}, Al^{3+})^{B}Ti^{4+}_{-2}$

In comparison to the Praborna roméite, the specimens from Fianel are richer in F, Na and Ti, and additionally contain significant amounts of Ce_2O_3 (up to 1.88 wt%) and Nb_2O_5 (up to 0.32 wt%; cf. Table 2, analysis 2). The IR-spectra of roméite from Fianel (Fig. 1b) and Praborna (Fig. 1a) are identical, except an absorption that is observed for the Praborna sample and is typical for the O-H vibration (arrow in Fig. 1a). This peak is missing in the Fianel roméite because it is, with exception of sample Se2.3, very rich in F, which almost completely fills the Y-site (Table 2, analysis 2). The myrmekitic Ti-rich roméite is rich in Ce_2O_3, Nb_2O_5, WO_3, As_2O_5 and UO_2 (Table 2, analysis 5). The low O value could indicate the presence of OH on the X-site.

The formula of the U-rich core of the crystal of Fig. 2c (Table 2, analysis 6) was calculated with Sb^{5+} because the mineral occurs within a roméite crystal and because the resulting stoichiometry does not correspond to any known mineral if all Sb is taken as Sb^{3+} (as e.g., in stibiobetafite (Ca, $Sb^{3+})_2(Ti^{4+}$, Nb, Ta)$_2O_6$(O, OH); Černý et al. 1979). The oxidation states of Fe and U are unknown, and were assumed as bivalent and tetravalent, respectively. The chemical formula obtained in this manner corresponds to the pyrochlore-group mineral betafite (Ca, $U)_{2-m}$(Ti, Nb, Ta)$_2O_6$(OH), with a high content of "roméite component." Due to the radiation damage induced by α-decay of U, many betafites are metamict (Hogarth 1961). No X-ray data could be collected on this 40 μm crystal. However, according to Lumpkin et al. (1994), a dose greater than 10^{16} alphas/mg gives a good indication that betafite is metamict. A minimum age of 30 Ma yields a dose of 1.6 10^{16} alphas/mg and thus suggests that the studied betafite is metamict, a

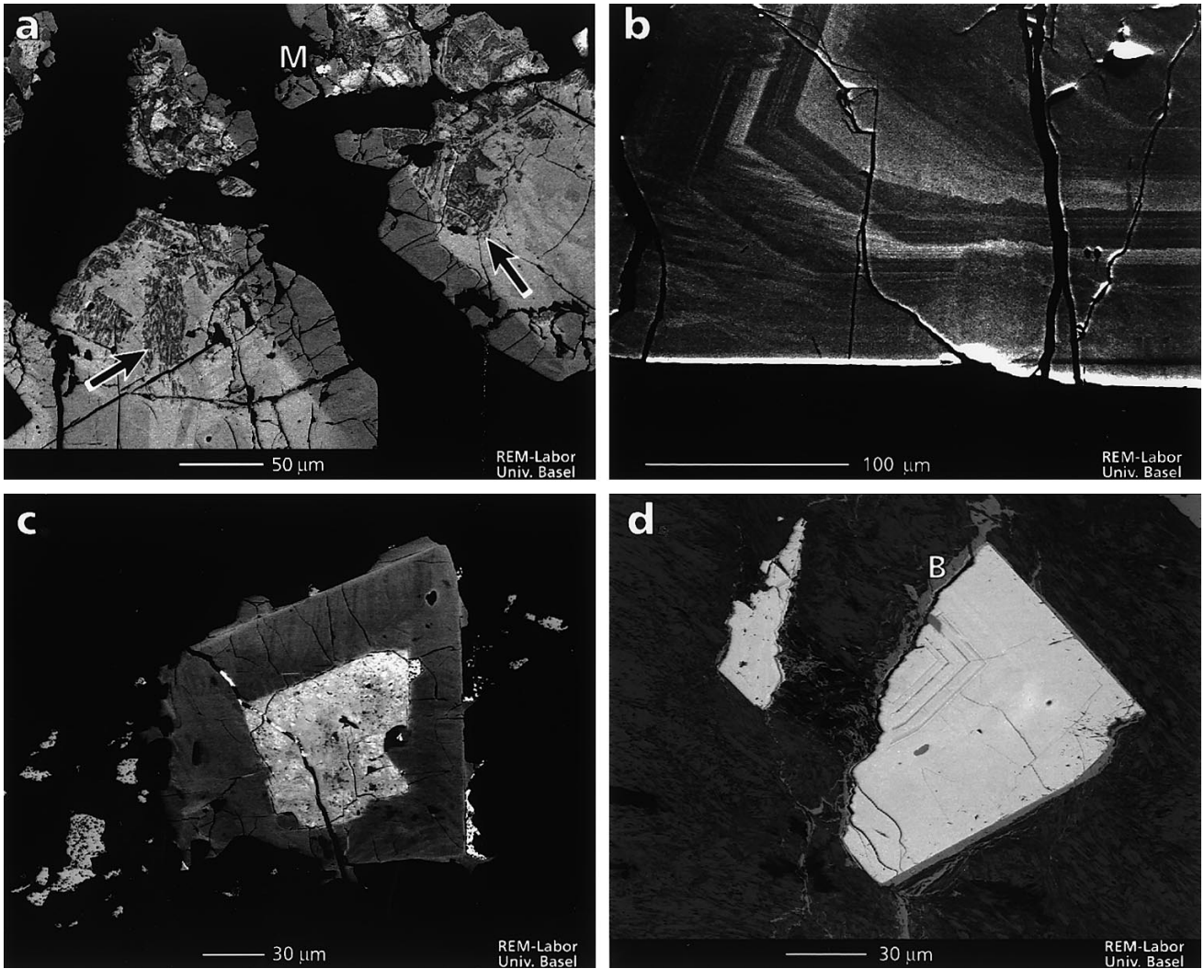

Fig. 2a–d BSE pictures of roméite from Val Ferrera, Switzerland. **a** Crystal from Fianel (sample Se2.4) displaying a dark, Ti-rich rim and containing dark, myrmekitic secondary roméite (*arrows*). *M* thorian monazite-(Ce) inclusion. **b** Roméite crystal (sample Se2.3) from Fianel, displaying oscillatory zonation. **c** Roméite crystal from Fianel with a core consisting of Sb-W-bearing betafite. **d** Broken, finely zoned crystal of roméite with narrow band of manganberzeliite (*B, intermediate grey*) in a johninnesite (*fibrous, dark grey*) veinlet from Schmorrasgrat

conclusion supported also by the porous appearance of the polished mineral surface. The low analytical totals may be due to the presence of H_2O on the A-site in addition to that on the Y-site, consistent with the DTA and DGA data of Hogarth (1961) which suggest coexistence of two types of H_2O-groups in betafite.

The chemical variability on the A- and B-sites can be described in terms of three end-members (Fig. 3a): (1) $^{A}Na^{A}Ca^{B}Sb_2O_6(F,OH)$, (2) $^{A}Ca_2{}^{B}Ti^{B}SbO_6(F,OH)$ and (3) $^{A}Ca_{1.5}{}^{A}\square_{0.5}{}^{B}Sb_2O_6(F,OH)$. These end-members are related to each other by the substitutions listed in Fig. 3a. The Fianel roméites lie between end-members (1) and (2); only the data for the oscillatory zoned sample Se2.3 (Fig. 2b) plot between (2) and (3) (cf. Table 2, analyses 3 and 4). Ce enters the roméite structure for example along exchange vector (d) $CeTi_2Na_{-1}Sb_{-2}$. The correlations observed in Fig. 3a and 3b correspond to an exchange vector (x) which can be written as (x) = (a) –2.6∗(b) – 0.7∗(d).

At *Schmorrasgrat* (Schams nappes), jacobsite-rich ores were discovered in 1994 by the senior author. Here, rare roméite crystals occur in post-S_1 veinlets which contain johninnesite, quartz and hematite. Some roméite crystals are broken, and at least some of the johninnesite crystallization takes place after this event (Fig. 2d). A narrow band of manganberzeliite marks the fracture. Roméite from Schmorrasgrat shows zonation patterns as fine bands (< 1 μm) aligned parallel to the growth surface (Fig. 2d).

Roméite from Schmorrasgrat (Table 2, analysis 11) differs from that of the other Val Ferrera occurrences by high contents of Fe_2O_3 (up to 3.08 wt%) and MnO (up to 8.09 wt%), by a low F content (< 0.38 pfu), and by the presence of significant amounts of As (up to 1 wt% As_2O_5). The low analytical totals are not well understood but may be due to small amounts of H_2O on the A-site (< 3 wt%). Fe has been calculated as Fe_2O_3 to account for the presence of hematite in the vein and to leave room for H_2O on the A-site. The analyses within the fine dark bands in Fig. 2d (Table 2, analysis 12) show enrichment of As_2O_5, Nb_2O_5 and Ce_2O_3 relative to rest of the crystal. The low analytical totals are probably related to an underestimation of Sb_2O_5, which could be due to topographic effects; the fine bands are softer than the enclosing roméite and appear as depressions on the polished sections.

The *Starlera* mine (Suretta nappe) furnished the only economic Mn-ores of Val Ferrera (braunite, exploited between 1918 and 1920; Heim and Tarnuzzer 1923). The associated Fe ores consist of hematite and quartz. Many post-S_1 veins (up to 30 cm thick) containing magnesian calcite, tilasite ($CaMgAsO_4F$), roméite and manganoan hydroxyl-phlogopite crosscut the ores. The roméite has a homogeneous appearance in BSE pictures except for some alteration, appearing as dark veinlets, dark diffusion fringes and dark crystal rims.

At Starlera, a Ti-poor and a Ti-rich roméite population can be distinguished (Table 2, analyses 9 and 10, respectively). Individual crystals of each population,

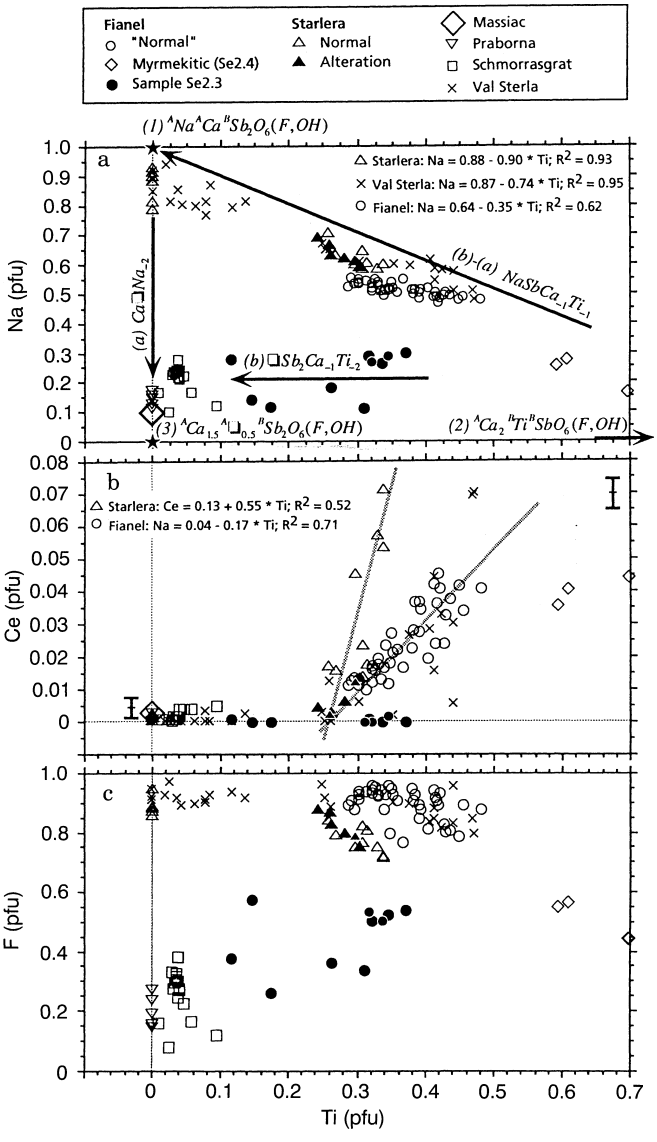

Fig. 3a–c Bivariable diagrams illustrating the crystal chemistry of the studied roméite samples ("lewisite" not shown). EMP data normalized to ΣB = 2. The estimated 1 σ errors for Ti resulting from counting statistics are 3% and 0.9% for 0.02 and 0.5 Ti pfu, respectively **a** Na vs Ti (pfu) diagram. Estimated 1 σ errors for Na resulting from counting statistics: 4% and 1.5% for 0.1 and 0.9 Na pfu, respectively **b** Ce vs Ti (pfu) diagram. The 1 σ errors for Ce resulting from counting statistics are plotted; the indicated linear correlations only consider analyses with Ti > 0.2 pfu, to account for the fact that Ce is enriched only above this critical Ti value. Note that correlation is not due to X-ray line interferences. **c** F vs Ti (pfu) diagram. 1 σ error for F resulting from counting statistics: 2% at 1 atom pfu level

however, are relatively homogeneous. The Ti-rich population contains up to 2.91 wt% Ce_2O_3 and 0.24 wt% Nb_2O_5. The variation observed within the Ti-rich population mainly takes place along (d) $CeTi_2Na_{-1}Sb_{-2}$, which would produce a slope of –1/2 on a Na vs. Ti plot (Fig. 3a,b); variation within the Ti-poor population is along vector (a). Alteration effects are only producing variation in As_2O_5 (up to 0.5 wt%), and the affected areas are similar in composition to the Ti-rich population.

The deposit of *Val Sterla* (Suretta nappe) contains one lens (~1 m) consisting of manganoan-magnesian calcite, roméite and quartz. The crystallization of these minerals took place during a static event that post-dates S_1. Fluorite occurs as idiomorphic crystals in vugs and represents an alteration product of the former paragenesis. Thin (< 5 μm) strips of a Sr-Al-As-(± P, S) mineral (kemmlitzite?) develop along some roméite grain boundaries and in fractures within roméite crystals. The roméite crystals from Val Sterla are characterized by pronounced oscillatory zoning (Fig. 4b, c). Under the petrographic microscope with crossed polarizers, some of the zones display a strong anisotropy (Fig. 4a). The growth zonation may be disturbed by post-crystallization phenomena: the rim of the crystal shown in Fig. 4b and 4c, for example, is replaced by Ti-poor roméite (see arrows). Similarly, a large portion of the crystal shown in Fig. 4d has been replaced.

The oscillatory zonation is mainly related to the coupled substitution $Na_2\square Sb_4Ca_{-3}Ti_{-4}$ (Fig. 5; Table 2, analyses N° 7 and 8). A Ce_2O_3 content up to 4.22 wt% is found in some zones where $TiO_2 > 7$ wt%, but no clear correlation exists between Ce and Ti (Fig. 3b). The replacing roméite (see e.g., Fig. 4d) is chemically similar to the roméite from the Ti-poor zones. In the crystal of Fig. 4d, the wavy appearance of the outer zone (1), the occurrence of a phantom of the primary zonation in the transformed zone (2), the rhythmical aspect of the replacement front (3), which suggests oscillatory reaction at a diffusion front (Ortoleva 1994), and the "fluidal" appearance of the disturbed area at (4), all indicate that this replacement was caused by a fluid after roméite crystallization.

Tripuhy

At Tripuhy (Minas Gerais, Brazil) mica schists grading into hematite schists (of probably synsedimentary exhalative origin) are crosscut by quartz veins with

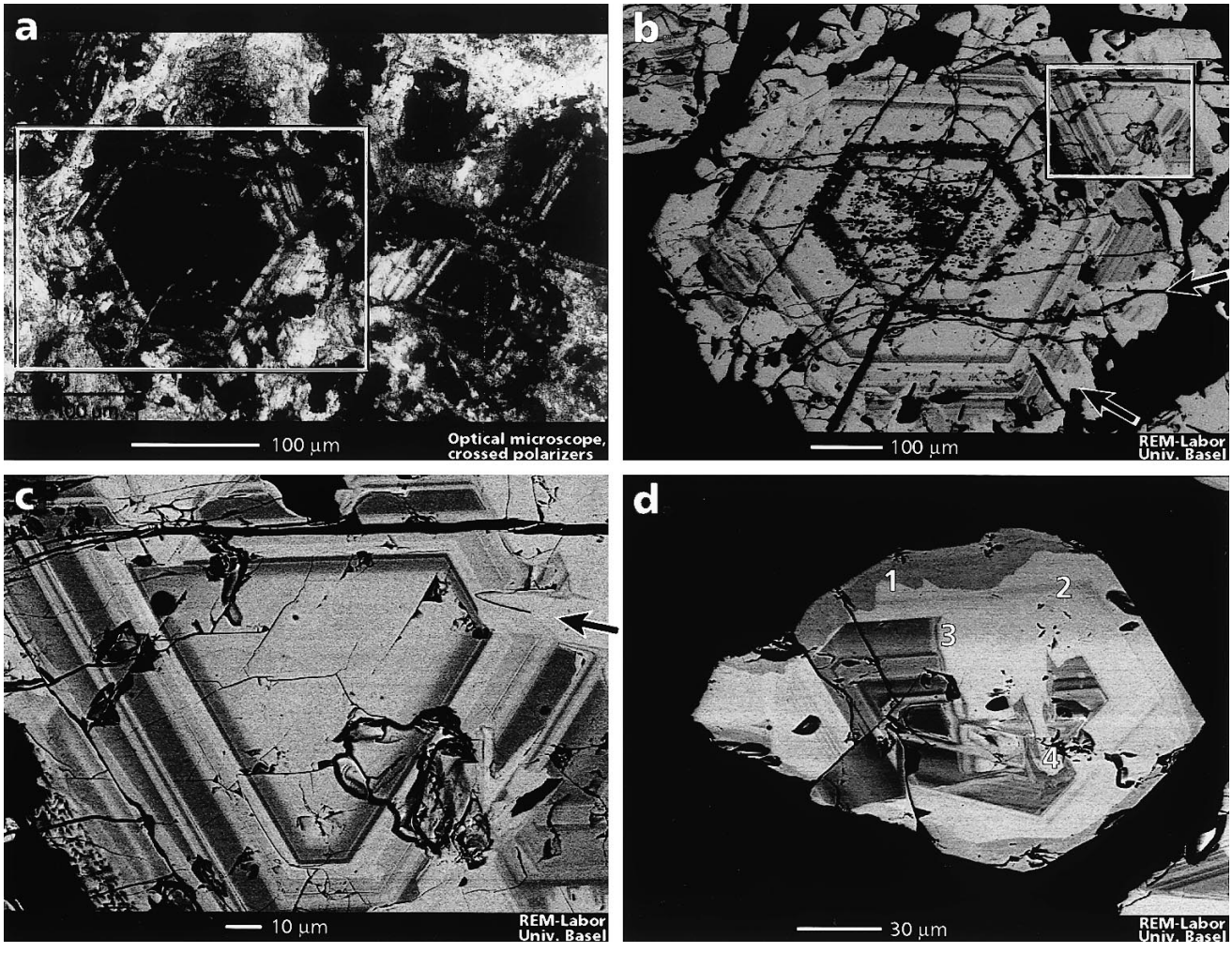

Fig. 4a–d Roméite from Val Sterla, Val Ferrera, Switzerland. **a** Photomicrograph of roméite-bearing sample; the location of Fig. 4b is indicated by the box; crossed polarizers. **b** BSE picture of a crystal with oscillatory zonation; the box corresponds to the view seen in Fig. 4c, and the *arrow* points to replacement textures along the rim of the crystal. **c** Detail of Fig. 4b; the *arrow* points to a replacement texture. **d** BSE picture of a zoned crystal with complex replacement textures

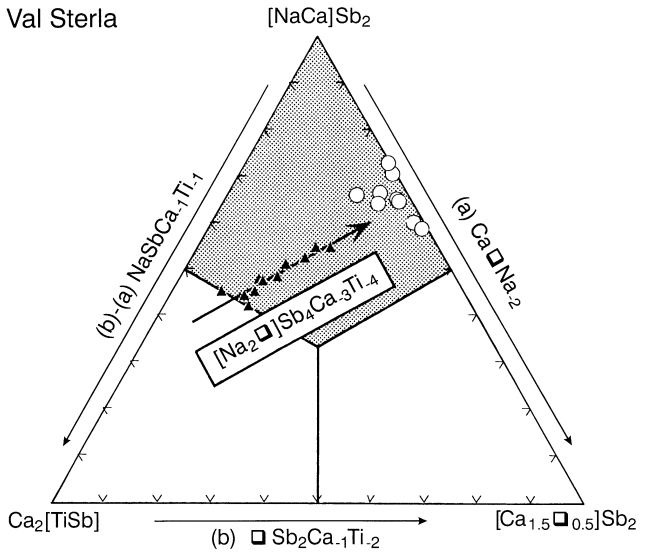

Fig. 5 Triangular plot $(NaCa)Sb_2$ – $Ca_2(TiSb)$ – $(Ca_{1.5}\square_{0.5})Sb_2$ displaying EMP-analyses of the zoned crystal shown in Fig. 4b (Val Sterla). *White circles* represent points measured in bright zones (low in Ti), *black triangles* designate points measured in dark zones (high in Ti)

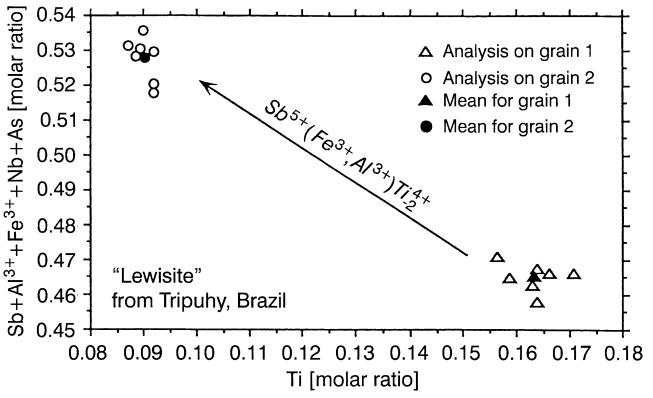

Fig. 6 $(Sb+Al^{3+}+Fe^{3+}+Nb+As)$ versus Ti (molar ratios) plot of EMP analyses of "lewisite" from Tripuhy, Brazil

cinnabar. Isolated "lewisite" crystals occur in alluvial sands originating from the mica schists, together with xenotime-(Y), monazite-(Ce), zircon, gold, tripuhyite and derbylite (Hussak and Prior 1895; Moore and Takaharu 1976). The 5 available "lewisite" crystals have inclusions of quartz, titanian hematite, and some phyllosilicates as identified by X-ray powder diffractometry. These inclusions exhibit a preferred orientation, indicating that "lewisite" postdates the formation of a schistosity.

The analyses of two different crystals (Table 2, analyses 13 and 14) show Al_2O_3, Nb_2O_5 and As_2O_5 up to 1.14, 0.24 and 0.94 wt%, respectively; Ce, Cl and F are below the microprobe detection limit, and H_2O is not present in significant quantity. Because hematite inclusions were observed, Fe has been assigned to the B-site as Fe^{3+}; another argument for this oxidation state is that exchange vector (e), which relates the compositions of the two grains (Fig. 6), requires the presence of a trivalent metal ion. The substitution (e) solely affects the B-site and is characterized by $Fe^{3+}/Al^{3+} \approx 2$. The contents of the A-site are very similar in both grains. "Lewisite" approximates the formula $(Ca, Mn, Na)_{2-m}(Sb, Ti, Al, Fe^{3+}, Nb, As^{5+})_2O_6$ where $m \approx 1$.

Hydrothermal veins

Roméite has also been reported from hydrothermal vein deposits such as, e.g., the fluorite-barite vein of Grube Clara, Germany (spherulitic roméite on barite and fluorite crystals; Walenta 1975), quartz-sulfides-carbonate veins in the Schneeberg complex, Austria (latest filling in cavities; Schaller 1916), and a quartz-stibnite vein at Massiac, France (Périchaud 1971).

At Massiac, roméite occurs as a cryptocrystalline, yellow alteration product of stibnite. It contains mainly Ca and Sb and only small amounts of Na_2O, FeO and Ce_2O_3 (< 1 wt% each), and is devoid of F (< 0.05 wt%; cf. Table 2, analysis 15). The low analytical total points to a H_2O content of approx. 13 wt%. In view of the findings of Ercit et al. (1994) for kalipyrochlore, H_2O is probably located on both the Y- and A-sites.

X-ray diffraction data for roméite and "lewisite"

Roméite from Praborna (containing 0.76 wt% F; see Table 2, analysis 1) shows d-values that are not listed on the JCPDS 27–89 card (Roméite, Långban, with 3.50 wt% F); these are located at 2.356 Å, 2.096 Å and 1.186 Å (Table 4).

Indexing the powder diagram of "lewisite" from Tripuhy could not be achieved as accurately as that of roméite; therefore, one sample was studied by single-crystal diffraction (Weissenberg and precession cameras). A cubic cell with $a = 10.29(2)$ Å was found, and systematic extinctions indicate the space group *Fd3m*. The cubic symmetry is also indicated by the octahedral shape of the crystals. Optically, however, the crystals are anisotropic and appear as aggregates of microscopic subgrains. This feature could be due to a phase transition similar to that observed at Alto do Giz pegmatite, Brazil, where parabariomicrolite occurs as an alteration product of microlite (Ercit et al. 1986); this transformation of the pyrochlore structure into a structure with hexagonal symmetry is explained as resulting from ordering of the A-site vacancies. A similar mechanism could possibly also explain the appearance of the Tripuhy "lewisite": some parts are transformed into a hexagonal phase, but most of it is still in the original cubic state.

Table 4 Powder diffraction data for roméite from Praborna and Fianel, and for "lewisite" from Tripuhy

					Roméite[b] Praborna (H41)			Roméite[b] Fianel (H40)			"Lewisite" Tripuhy, JCPDS 7-66 cubic hexagonal			
		h	k	l	$d_{meas.}$	I/I_0	d_{calc}	$d_{meas.}$	I/I_0	d_{calc}	$d_{meas.}$	I/I_0	d_{calc}	d_{calc}
1	[a]	1	1	1	5.940	38	5.932	5.931	37	5.931	5.84	20	5.94	5.87
2	[a]	1	1	3	3.100	28	3.098	3.097	40	3.097	3.08	30	3.1	3.08
3	[a]	2	2	2	2.968	100	2.966	2.965	100	2.965	2.94	100	2.97	2.93
4	[a]	0	0	4	2.570	20	2.569	2.568	33	2.568	2.55	30	2.57	2.54
5		3	3	1	2.356	6	2.357							
6		4	2	2	2.096	2	2.097							
7	[a]	3	3	3	1.978	23	1.977	1.977	15	1.977	1.966	30	1.980	1.971
9	[a]	0	4	4	1.817	45	1.816	1.816	67	1.816	1.813	100	1.819	1.813
10	[a]	1	3	5	1.737	9	1.737	1.736	12	1.736	1.734	30	1.739	1.736
11	[a]	3	3	5	1.567	6	1.567	1.567	8	1.566				
12	[a]	2	2	6	1.549	39	1.549	1.549	56	1.549	1.548	100	1.551	1.552
13	[a]	4	4	4	1.483	9	1.483	1.483	14	1.483	1.483	30	1.485	1.481
14	[a]	1	5	5	1.439	7	1.439	1.438	10	1.438	1.438	30	1.441	1.436
15	[a]	3	5	5	1.337	9	1.338	1.337	13	1.337	1.337	30	1.339	1.337
16	[a]	0	0	8	1.284	6	1.284	1.284	11	1.284	1.284	30	1.286	1.287
17		7	5	1	1.186	3	1.186							
18	[a]	6	6	2	1.178	15	1.178	1.178	24	1.178	1.179	50	1.180	1.794
19	[a]	8	4	0	1.148	13	1.149	1.148	21	1.148	1.150	50	1.150	1.154
20											1.127	20	1.129	1.127
21					$a = 10.2739(8)$			$a = 10.2720(1)$			1.103	10	1.109	1.103
22											1.078	20	1.079	1.077
23											1.050	50	1.050	1.050
24											1.033	20	1.034	1.033
25											0.996	30	0.995	0.997
26											0.989	50	0.986	0.988
													$a = 10.29(2)$	$a = 7.323(3)$ $c = 17.61(1)$

[a] Line indexed in JCPDS 27-89 (roméite, Långbam).
[b] Guinier Camera, Cu-K_α, Ni-filtered.

Discussion

Geology of roméite

As described above, roméite is formed at different conditions in two very different geological environments: (1) in metamorphosed Mn-deposits during the *retrograde metamorphism*, and (2) in hydrothermal vein deposits during *late hydrothermal* stages or during *weathering*. Type (1) includes the famous deposits of Långban and Jakobsberg in Vermland, Sweden (Boström et al. 1979). All roméite-bearing Mn-deposits described in this paper are most likely of synsedimentary exhalative origin. We therefore conclude that such a geochemical environment is favorable for roméite crystallization during metamorphism. Roméite thus can be taken as a good indicator for the synsedimentary exhalative origin of a metamorphosed Mn-deposit.

Crystal chemistry

The A- and B-site contents of roméite from the deposits of Val Ferrera and Praborna can be described in terms of three hypothetical end-members which are related to each other by three substitutions (see Fig. 3a). Compositions near (3) $^{A}Ca_{1.5}{}^{A}\square_{0.5}{}^{B}Sb_2O_6(F,OH)$ and (1) $^{A}Na^{A}Ca^{B}Sb_2O_6(F,OH)$ were identified, but no more than 60% of (2) $ACa_2{}^{B}Ti^{B}SbO_6(F,OH)$ component were observed. Only one grain from Fianel was found to lie along vector (b). Moreover, a large compositional gap appears between end-members (1) and (3) along vector (a). The two "lewisite" grains studied differ in the composition of the B-site [vector (e)].

Ce enters the roméite structure mainly along (d) $^{A}Ce^{B}Ti_2{}^{A}Na_{-1}{}^{B}Sb_{-2}$ at Starlera and along a linear combination of vectors (a), (b) and (d) at Fianel. The role of H_2O is not important on the A-site in the samples from metamorphosed deposits; only at Schmorrasgrat a limited amount may be present. The situation is different for roméite formed in sulfide veins, as it contains significant amounts of water (about 13 wt%) and a relatively high cation vacancy on the A-site.

The Y-site in roméite has a composition that is distinct for each deposit. Hydroxyl is dominant at Praborna, whereas fluorine dominates at Fianel (Fig. 3c); the Y-site of "lewisite" from Tripuhy is vacant. At Praborna, substantial amounts of O appear to enter the Y-site along (c) $^{A}Na^{Y}(OH)^{A}(M^{2+})_{-1}{}^{Y}O_{-1}$.

Betafite is typically found in igneous rocks, mainly carbonatites and pegmatites (cf. Kennedy 1979; Lumpkin and Ewing 1985, 1996), and its occurrence in a sediment-hosted metamorphosed deposit is very unusu-

al. Moreover, this is the first documentation of substantial amounts of Sb^{5+} in betafite which additionally is very rich in Ti (cf. data of Hogarth 1977).

Nomenclature and "lewisite" status

The fact that roméite from different localities, each of which has a distinct geological history, displays contrasting chemical compositions, requires a more differentiated nomenclature. A simple way to account for this variability is to indicate the dominant Y-site species using a prefix such as hydroxyl-, fluor- or "Y-vacant-". Note that in the pyrochlore-group s.l. (Aleph Computer 1995), no IMA-accepted species is given with F as dominant anion on the Y-site. In the literature, however, pyrochlore group minerals dominated by F have been described (e.g., Lumpkin and Ewing 1985, pyrochlore with 3.30 wt% F). A more complete, albeit complex way, would be to take into account structural end-members based on the A-site occupancy (see Fig. 7). Generally speaking, roméite should be assigned a subgroup status within the pyrochlore group. Ce and Nb are typical elements in the pyrochlore s.s. minerals, and an intermediate composition between betafite and roméite has been discovered at Fianel (Table 2, analysis 6).

Our data suggest that "lewisite" is a mixture of roméite and a phase which is structurally related to pyrochlore and develops at the expense of roméite.

Alteration

Alteration is the main factor controlling the A-site vacancies in pyrochlore s.s.: leaching of Na is typically observed during "primary" alteration (hydrothermal conditions), whereas a trend towards high degree of A-site cation vacancy is typical for "secondary" alteration (near-surface conditions; Lumpkin and Ewing 1992, 1995). Lumpkin and Mariano (1996), however, recently documented that the conditions during crystallization may sometimes also control the A-site vacancies (e.g., in carbonatites).

In roméite from Val Ferrera, the altered zones are characterized, relative to the undisturbed matrix, by higher Ce, Nb, W, As and U contents, by a higher Ti content negatively correlated to Na, and by a lower F content. This type of alteration is similar to the "primary" alteration defined in pyrochlores s.s. (arrow in Fig. 7).

The roméite from hydrothermal veins (e.g. Massiac) and "lewisite" display high cation vacancies on the A-site. This is not the result of "secondary" alteration, but it reflects special conditions during crystallization.

Implications for element mobility in the deposits of Val Ferrera

The complex crystal chemistry of roméite records characteristics of the fluid chemistry during mineral growth and subsequent alteration. For example, at Schmorrasgrat, roméite is an accessory vein mineral whose chemical composition (As- and Mn-rich) is related to the dominant vein mineral (johninnesite).

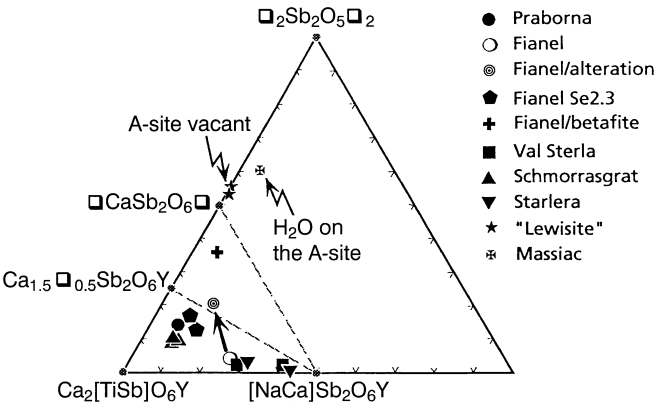

Fig. 7 Triangular plot of EMP analyses of Table 2 displaying the chemical composition of the A-site. Note that the A-site "vacancies" (□) may host H_2O-groups (cf. also Table 1). The *arrow* shows the alteration trend for the roméite from Fianel (corresponding to "primary" alteration of Lumpkin and Ewing 1992)

The correlation between Ti and Ce in roméite is different for each locality and generation (Fig. 3b); moreover, Ce is enriched only if Ti > 0.2 atoms pfu. The good positive correlations between Ce and Ti at Fianel and Starlera indicate that a similar trend existed also in the fluid. At Fianel, the data further suggest that the activities of Ti and Ce in the fluid increase during the crystallization of roméite. The poor correlation between Ce and Ti for the Val Sterla samples, suggesting disequilibrium between fluid and rock, supports the interpretation of the oscillatory zoning as the result of geochemical self-organization (Ortoleva 1994). At Val Sterla, the replacing roméite has chemical and textural features similar to the primary roméite, suggesting that its formation could be related to the same fluid that produced the primary roméite.

This study of the crystal chemistry of roméite supports the observation of Gieré (1990), that Ti and REE often migrate together in hydrothermal environments. Moreover, it allows to recognize mobility of Nb, W, As, V in the ores of Val Ferrera during roméite alteration at lower greenschist facies conditions.

Acknowledgements We wish to thank Claire Prospert (Inst. of Mineralogy, Fribourg, Switzerland), who sacrificed some of her holidays in Brazil to collect "lewisite" samples, to Paulo Anselmo Matioli (University of Sao Paulo, Brazil) who helped her in her quest, and to Prof. Cesar Mendonça Ferreira (University of Ouro Preto, Brazil) who finally provided the 5 "lewisite" crystals. The sample from Massiac was provided by the Naturhistorisches Museum of Basel, and the samples from Praborna by the Musée de Géologie in Lausanne (Switzerland) and by Franco Vanini, Varese (Italy). This work benefited from helpful suggestions of Gregory Lumpkin (Australian Nuclear Science and Technology Organization, Menai, Australia) and Peter Berlepsch (Mineralogisch-Petrographisches Institut, Universität Basel). Our gratitude is also extended to François Bussy (EMP laboratory, Université de Lau-

sanne), Susanne Schmidt (EMP laboratory, Universität Basel) and Richard Guggenheim (SEM laboratory, Universität Basel) for giving us access to their laboratories, and to Daniel Mathys (SEM laboratory, Universität Basel) for the BSE images. This work was supported by the Swiss National Science Foundation (grants n° 2000–43350.95 and 2124–042200.94).

References

Aleph Computer SA (1995) Mineral, version 95.2

Boström K, Rydell H, Joensuu O (1979) Långban – an exhalative sedimentary deposit ? Econ Geol 74: 1002–1011

Brandenberger E (1931) Die Kristallstruktur von Koppit. Z Kristallogr 76: 322–334

Brugger J (1995) Mineralogy of the iron-manganese deposit of Fianel, Val Ferrera, GR. Schweiz Mineral Petrogr Mitt 75: 296–297

Brugger J (1996) The Fe, Mn, (V, Sb, As, Be, W) deposits of Val Ferrera (Graubünden, Switzerland). PhD thesis, Institute for Mineralogy and Petrography, Basel, Switzerland

Brugger J, Cabalzar W, Weibel M (1994) Neufund: Romeit in den Schweizer Alpen. Mineralienfreund 4: 1–7

Brugger J, Groberty B, Gieré R (1995) As-Y-rich scheelite-powellite from Fianel (Val Ferrera, Graubünden, Switzerland). Terra Abstracts (suppl N° 1 to Terra Nova 7): 291

Černý P, Hawthorne FC, Laflame JHG, Hinthorne JR (1979) Stibiobetafite, a new member of the pyrochlore group from Vezna, Czechoslovakia. Can Mineral 17: 583–588

Damour A (1841) Sur la roméite, nouvelle espèce minérale, de St. Marcel, Piemont. Annales des Mines 20 (3): 247

Dana D. Dana ES (1951) The system of mineralogy. (7th edn, rewritten and enlarged by C. Palache, H. Berman, C. Frondel). Wiley, New York

Ercit TS, Robinson GW (1994) A refinement of the structure of ferritungstite from Kalzas Mountains, Yukon, and observations on the tungsten pyrochlores. Can Mineral 32: 567–574

Ercit TS, Hawthorne FC, Černý P (1986) Parabariomicrolite, a new species and its structural relationship to the pyrochlore group. Can Mineral 24: 655–663

Ercit TS, Hawthorne FC, Černý P (1994) The structural chemistry of Kalipyrochlore. Can Mineral 32: 417–420

Fleischer M (1993) Glossary of mineral species. The Mineralogical Record, Tucson

Gaertner HRv (1930) Die Kristallstrukturen von Loparit und Pyrochlor. Neues Jahrb Mineral Beilage-Band 61, Abt A: 1–30

Gieré R (1990) Hydrothermal mobility of Ti, Zr and REE: examples from the Bergell and Adamello contact aureoles (Italy). Terra Research 2: 60–67

Godard C, Chat C (1994) Petrocalc: a petrological software to manage relational database of chemical analyses. IMA 94 book of abstracts, International Mineralogical Association, Pisa: 147

Heim A, Tarnuzzer C (1923) Die Eisen-Manganerzlagerstätten im Val Ferrera. Beitr Geol Schweiz Geotech Ser 13/1

Hogarth DD (1977) The pyrochlore group. Am Mineral 62: 403–410

Hogarth DD (1961) A study of pyrochlore and betafite. Can Mineral 6: 610–633

Hussak E, Prior GT (1895) Lewisite and zirkelite, two new Brazilian minerals. Mineral Mag 11: 80–88

Kennedy I (1979) Some interesting radioactive minerals from the Bancroft area, Ontario, Canada. Mineral Rec 10: 153–158

Lumpkin GR, Ewing RC (1985) Natural pyrochlores: analogues for actinide host phases in radioactive waste forms. In: Jantzen CH, Stone JA, Ewing RC (eds) Scientific basis for nuclear waste management VIII, Materials Research Society Symposium Proceedings, vol. 44, p. 647–654. Materials Research Society, Pittsburgh, Pennsylvania

Lumpkin GR, Ewing RC (1992) Geochemical alteration of pyrochlore group minerals: microlite subgroup. Am Mineral 77: 179–188

Lumpkin GR, Ewing RC (1995) Geochemical alteration of pyrochlore group minerals: pyrochlore subgroup. Am Mineral 80: 732–743

Lumpkin GR, Ewing RC (1996) Geochemical alteration of pyrochlore group minerals: betafite subgroup. Am Mineral 81: 1237–1248

Lumpkin GR, Mariano AN (1996) Natural occurrences and stability of pyrochlore in carbonatites, related hydrothermal systems, and weathering environments. In: Murphy WM, Knecht DA (eds) Scientific basis for nuclear waste management XIX, Materials Research Society Symposium Proceedings, vol. 412, p. 612–619. Materials Research Society, Pitts burgh, Pennsylvania

Lumpkin GR, Hart KP, McGlinn PJ, Payne TE, Gieré R, Williams CT (1994) Retention of actinides in natural pyrochlores and zirconolites. Radiochim Acta 66/67: 469–474

Martin-Vernizzi S (1984) La mine de Praborna (Val d'Aoste, Italie): une série manganèsifère métamorphisée dans le faciès éclogite. PhD thesis, Université Pierre et Marie Curie, Paris

Moore PB, Takaharu A (1976) Derbylite $Fe_4^{3+}Ti_3^{4+}Sb^{3+}O_{13}(OH)$, a novel close-packed oxide structure. Neues Jahob Mineral Abh 126: 292–303

Natta G, Baccaredda M (1933) Tetrossido di antimonio e antimoniati. Z Kristallogr 85: 271–296

Ortoleva PJ (1994) Geochemical self organisation. Oxford University Press, Oxford, New York, Toronto

Périchaud J-J (1971) Les gisements metalliques du district à antimoine de Brioude-Massiac (Massif Central français). Bull Bur Rech Geol Min serie 2, section II, 2: 1–55.

Ringwood AE, Kesson SE, Reeve KD, Levins DM, Ramm EJ (1988) Synrock. In: Lutze W, Ewing RC (eds) Radioactive waste forms for the future. North-Holland, Amsterdam: 233–334

Schaller WT (1916) Mineralogical notes. Schneebergite and roméite. US Geol Surv Bull 610: 81–95

Schmid SM, Rück P, Schreurs G (1990) The significance of the Schams nappes for the reconstruction of the paleotectonic and orogenic evolution of the Penninic zone along the NFP-20 East traverse (Grisons, eastern Switzerland). Mém Soc géol Fr 156: 263–287

Schreurs G (1993) Structural analysis of the Schams nappes and adjacent tectonic units: implications for the orogenic evolution of the Penninic zone in Eastern Switzerland. Bull Soc géol Fr 164: 415–135

Stormer JCJ, Pierson ML, Tacker RC (1993) Variation of F and Cl X-ray intensity due to anisotropic diffusion in apatite during electron microprobe analysis. Am Mineral 78: 641–648

Stucky K (1960) Die Eisen- und Manganerze in der Trias des Val Ferrera. Beitr Geol Schweiz Geotech Ser 37

Trümpy R (1980) Geology of Switzerland, a guide book. Part. A. An outline of the geology of Switzerland. Schweizerische geologische Kommission, Wepf, Basel

Van Wambeke L (1978) Kalipyrochlore, a new mineral of the pyrochlore group. Am Mineral 63: 528–530

Walenta K (1975) Die Sekundärmineralien des Schwerspatganges der Grube Clara bei Oberwolfach im mittleren Schwarzwald. Aufschluss 26: 369–411

Zedlitz O (1932) Die Kristallstukturen von Romeit und Schneebergit. Z Kristallogr 81: 253–263